



PRIFYSGOL  
**BANGOR**  
UNIVERSITY

## Is there a tectonically driven super-tidal cycle?

Green, Mattias; Molloy, Joseph; Davies, Hannah; Duarte, Joao

### Geophysical Research Letters

DOI:

[10.1002/2017GL076695](https://doi.org/10.1002/2017GL076695)

Published: 11/04/2018

Peer reviewed version

[Cyswllt i'r cyhoeddiad / Link to publication](#)

*Dyfyniad o'r fersiwn a gyhoeddwyd / Citation for published version (APA):*

Green, M., Molloy, J., Davies, H., & Duarte, J. (2018). Is there a tectonically driven super-tidal cycle? *Geophysical Research Letters*, 45(8), 3568-3576. <https://doi.org/10.1002/2017GL076695>

#### Hawliau Cyffredinol / General rights

Copyright and moral rights for the publications made accessible in the public portal are retained by the authors and/or other copyright owners and it is a condition of accessing publications that users recognise and abide by the legal requirements associated with these rights.

- Users may download and print one copy of any publication from the public portal for the purpose of private study or research.
- You may not further distribute the material or use it for any profit-making activity or commercial gain
- You may freely distribute the URL identifying the publication in the public portal ?

#### Take down policy

If you believe that this document breaches copyright please contact us providing details, and we will remove access to the work immediately and investigate your claim.

# Is there a tectonically driven super-tidal cycle?

J. A. M. Green<sup>1</sup>, J. L. Molloy<sup>1,2</sup>, H. S. Davies<sup>3,4</sup>, and J. C. Duarte<sup>3,4,5</sup>

<sup>1</sup>School of Ocean Sciences, Bangor University, Menai Bridge, UK

<sup>2</sup>Department of Geography, University of Sheffield, Sheffield, UK

<sup>3</sup>Departamento de Geologia, Faculdade de Ciências, Universidade de Lisboa, Lisbon, Portugal

<sup>4</sup>Instituto Dom Luiz (IDL), Faculdade de Ciências, Universidade de Lisboa, Lisbon, Portugal

<sup>5</sup>School of Earth, Atmosphere and Environment, Monash University, Melbourne, Australia

## Key Points:

- Earth is in a semi-diurnal tidal maximum and will go through another during the supercontinent cycle
- The average dissipation rates over the supercontinent cycle are lower than present rates
- This highlights a deep-time cycle of importance for past and future Earth system studies

---

Corresponding author: Dr Mattias Green, [m.green@bangor.ac.uk](mailto:m.green@bangor.ac.uk)

**Abstract**

Earth is 180 Myr into the current Supercontinent cycle and the next Supercontinent is predicted to form in 250 Myr. The continuous changes in continental configuration can move the ocean between resonant states, and the semi-diurnal tides are currently large compared to the past 252 Myr due to tidal resonance in the Atlantic. This leads to the hypothesis that there is a “super-tidal” cycle linked to the Supercontinent cycle. Here, this is tested using new tectonic predictions for the next 250 Myr as bathymetry in a numerical tidal model. The simulations support the hypothesis: a new tidal resonance will appear 150 Myr from now, followed by a decreasing tide as the supercontinent forms 100 Myr later. This affects the dissipation of tidal energy in the oceans, with consequences for the evolution of the Earth-Moon system, ocean circulation and climate, and implications for the ocean’s capacity of hosting and evolving life.

**1 Introduction**

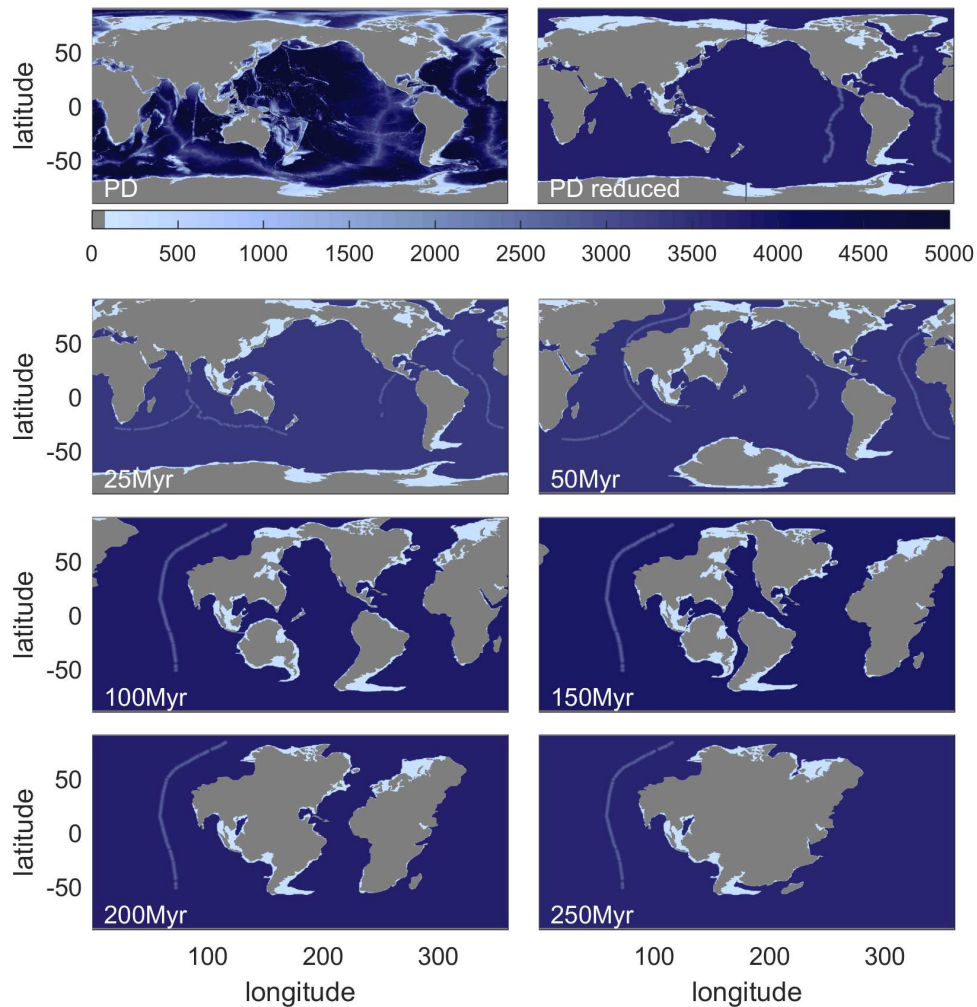
The Earth moves through a cyclic dispersion and aggregation of supercontinents over a period of 400–500 Myr, in what is known as the Supercontinent cycle [Nance *et al.*, 1988; Rogers and Santosh, 2003; Matthews *et al.*, 2016]. Pangea, the latest supercontinent, broke up around 180 Ma [Golonka, 1991, 2007] and it is predicted that a new supercontinent will form over the next 200–250 Myr [e.g., Yoshida and Santosh, 2011; Duarte *et al.*, 2018]. The break up of a supercontinent may lead to the formation of several internal oceans that will grow and eventually close. The lifecycle of each of these oceans is known as the Wilson Cycle [Wilson, 1966; Burke and Dewey, 1974]. Consequently, the completion of a Supercontinent cycle through the formation of a supercontinent is generally preceded by the termination of several Wilson cycles [e.g., Burke, 2011]. There is strong evidence that the tides are currently unusually large and that, for most of the current supercontinent cycle, they have been less energetic than at present [Kagan and Sundermann, 1996; Green *et al.*, 2017]. The exception is the past 2 Myr, during which the continental configuration has led to a tidal resonance in the Atlantic [e.g., Platzman, 1975; Green, 2010]. This (near-)resonant state has led to increased global tidal dissipation rates, which were further enhanced during glacial low stands in sea-level [Egbert *et al.*, 2004; Arbic and Garrett, 2010; Griffiths and Peltier, 2008; Green, 2010; Wilmes and Green, 2014; Green *et al.*, 2017]. An ocean basin can house resonant tides when the width of the basin,  $L$  is equal to a multiple of half-wavelengths,  $\lambda = \sqrt{gHT}$  ( $T$  is the tidal period,

47  $g$  is gravity, and  $H$  is water depth) of the tidal wave. Because today's resonant basin, the  
48 Atlantic, is currently opening we would expect it to move away from the resonant state  
49 as it continues to widen, if we assume that the water depth and tidal period remain con-  
50 stant. Later on during the Supercontinent cycle, we would expect either another basin to  
51 become resonant, either the Pacific if the Atlantic continues to open, or the Atlantic to be-  
52 come resonant again if it starts to close. This leads us to ask two questions: i) when and  
53 where does this second resonance occur, if at all, and ii) is there a super-tidal cycle, i.e.,  
54 a cycle in the tidal amplitudes, associated with the supercontinent cycle? Here, the ques-  
55 tions will be answered by new simulations of the possible evolution of the tide over the  
56 next 250 Myr. This is done by implementing the tectonic scenario in *Duarte et al.* [2018]  
57 as the bathymetric boundary condition in the tidal model described by *Green et al.* [2017].

63 *Duarte et al.* [2018] describe one possible scenario for the formation of the next su-  
64 percontinent, Aurica, 250 Myrs into the future. Aurica is predicted to be fairly circular  
65 and located in the present day equatorial Pacific Ocean [see *Duarte et al.*, 2018, and our  
66 Fig. 1]. It is formed by the closure of both the present day Atlantic and Pacific Oceans,  
67 which can only happen if a new ocean opens up. In the scenario, a bisection of Eura-  
68 sia leads to the formation of a new ocean basin via intracontinental rifting. The motiva-  
69 tion for the double-basin closure is that both the Atlantic and the Pacific oceanic litho-  
70 spheres are already, in some regions, 180 Ma old [although the Pacific oceanic basin is  
71 much older; *Golonka*, 1991; *Müller et al.*, 2008; *Boschman and van Hinsbergen*, 2016],  
72 and oceanic plates older than 200 Ma are rare in the geological record [*Bradley*, 2011].  
73 Consequently, it can be argued that both the Pacific and Atlantic must close to form the  
74 new supercontinent

75 Changes in the tides, and the associated tidal dissipation rates, on geological time  
76 scales have had profound implications for the Earth system. *Herold et al.* [2012] and *Green*  
77 *and Huber* [2013] show that the changed location of abyssal tidal dissipation during the  
78 Eocene (55 Ma) can explain the reduced meridional temperature gradients seen in the  
79 proxy record for sea-surface temperature that coupled climate models have struggled to re-  
80 produce [see *Herold et al.*, 2012, for a summary]. Furthermore, the reduced tidal dissipa-  
81 tion during the Mesozoic and Cenozoic eras reported by *Green et al.* [2017] had implica-  
82 tions for lunar recession rates, and hence for interpreting cyclostratigraphy and long-term  
83 climate cycles [*Waltham*, 2015], for the evolution of the Earth-Moon system [*Green et al.*,  
84 2017], and for the evolution of life [*Balbus*, 2014].

85 The disposition of the continents on Earth over geological time scales consequently  
 86 has a direct and major impact in the evolution of the Earth-Moon System, and tidal dissipation should be included in global ocean- and climate models, especially over long-time-  
 87 scales [Green and Huber, 2013]. The overall aim of this paper is to evaluate if there is a  
 88 super-tidal cycle linked to the Supercontinent cycle. We do this by expanding the work of  
 89 Green *et al.* [2017] by adding tidal simulations 250 Myr into the future using the tectonic  
 90



58 **Figure 1.** Shown is the tectonic evolution and eventual formation of the next supercontinent, Aurica. The  
 59 top two panels show present day (PD) and PD reduced bathymetries, respectively (see methods for details).  
 60 The timings for the other slices are noted in the lower left corner of each panel. The colours mark the depths  
 61 used in the tidal model simulations: light blue is 200 m, intermediate blue is 2500 m, and the majority of the  
 62 ocean is less than 4000 m deep (see methods below for details).

91 predictions in *Duarte et al.* [2018] as bathymetric boundary conditions. Consequently, this  
 92 paper will increase our fundamental understanding of the Earth system, and it will, if the  
 93 hypothesis is correct, lead to a first-order predictability of when large supertides may oc-  
 94 cur in Earth’s history. To obtain this knowledge, we want to cover a full supercontinent  
 95 cycle to see if there is a super-tidal cycle. The logical thing to do is to expand the super-  
 96 continent cycle we are currently in into the future, because the first part of it has already  
 97 been covered and shown to be tidally less energetic than PD [*Green et al.*, 2017]. In the  
 98 next section we describe the tidal model and the bathymetric time-slices used to obtain the  
 99 results in section 3. Section 4 closes the paper with a discussion and conclusions, and an  
 100 outlook in to further work.

## 101 2 Modelling future tides

### 102 2.1 Tides

103 We use OTIS – the Oregon State University Tidal Inversion Software – to simulate  
 104 the evolution of the future tides. OTIS is a portable, dedicated, numerical shallow water  
 105 tidal model, which has been used extensively for both global and regional modelling of  
 106 past, present and future ocean tides [e.g., *Egbert et al.*, 2004; *Green*, 2010; *Pelling and*  
 107 *Green*, 2013; *Green and Huber*, 2013; *Wilmes and Green*, 2014; *Green et al.*, 2017]. It is  
 108 highly accurate both in the open ocean and in coastal regions [*Stammer et al.*, 2014], and  
 109 it is computationally efficient. The model solves the linearised shallow-water equations  
 110 [e.g., *Hendershott*, 1977]:

$$\frac{\partial \mathbf{U}}{\partial t} + \mathbf{f} \times \mathbf{U} = -gH\nabla(\zeta - \zeta_{EQ} - \zeta_{SAL}) - \mathbf{F} \quad (1)$$

$$\frac{\partial \zeta}{\partial t} = -\nabla \cdot \mathbf{U} \quad (2)$$

111 Here  $\mathbf{U}$  is the depth integrated volume transport (i.e., tidal current velocity  $\mathbf{u}$  times water  
 112 depth  $H$ ),  $f$  is the Coriolis vector,  $g$  denotes the gravitational constant,  $\zeta$  is the tidal ele-  
 113 vation and  $\zeta_{SAL}$  denotes the tidal elevation due to self-attraction and loading (SAL), and  
 114  $\zeta_{EQ}$  is the equilibrium tidal elevation. For simplicity we used a constant SAL correction  
 115 with  $\beta = 0.1$  [*Egbert et al.*, 2004].  $\mathbf{F}$  represents energy losses due to bed friction and tidal  
 116 conversion. The former is represented by the standard quadratic law:

$$\mathbf{F}_B = C_d \mathbf{u} |\mathbf{u}| \quad (3)$$

117 where  $C_d = 0.003$  is a drag coefficient, and  $\mathbf{u}$  is the total velocity vector for all the tidal  
 118 constituents. The conversion,  $\mathbf{F}_w = C|\mathbf{U}|$ , includes a conversion coefficient  $C$ , which is

119 here defined as [Zaron and Egbert, 2006; Green and Huber, 2013]

$$C(x, y) = \gamma \frac{(\nabla H)^2 N_b \bar{N}}{8\pi^2 \omega} \quad (4)$$

120 Here,  $\gamma = 50$  is a scaling factor,  $N_b$  is the buoyancy frequency at the sea-bed,  $\bar{N}$  is the  
 121 vertical average of the buoyancy frequency, and  $\omega$  is the frequency of the tidal constituent  
 122 under evaluation. The buoyancy frequency is given by  $N = N_0 \exp(-z/1300)$ , where  
 123  $N_0 = 5.24 \times 10^{-3} \text{ s}^{-1}$  and based on a least squares fit to present day climatology values  
 124 [Zaron and Egbert, 2006]. The future stratification is obviously unknown, and to estimate  
 125 potential effects of altered stratification we did a set of sensitivity simulations in which  $C$   
 126 was doubled or halved. As in other tidal simulations this had a relatively minor effect on  
 127 the global tides, and we will not discuss these results further [see, e.g., Egbert *et al.*, 2004;  
 128 Green and Huber, 2013].

129 The model solves equations (1)–(2) using the astronomic tide generating force as  
 130 the only forcing (represented by  $\zeta_{EQ}$  in Eq. (1)). An initial spin-up from rest of over 7  
 131 days is followed by a further 5 days of simulation time, on which harmonic analysis is  
 132 performed to obtain the tidal elevations and transports. Here, we focus on the  $M_2$  and  $K_1$   
 133 constituents only.

## 134 **2.2 Bathymetry data**

### 135 **2.2.1 Present Day bathymetries**

136 The Present Day (PD) bathymetry is the same as in Green *et al.* [2017]: see our  
 137 Fig. 1, top left panel. To avoid open boundaries, the equilibrium tide was used as forc-  
 138 ing at  $88^\circ$  when appropriate. Tests with a vertical wall at the poles (not shown) did not  
 139 change the results. All simulations were done with  $1/4^\circ$  horizontal resolution. The PD  
 140 control simulation was compared to the elevations in the TPXO8 database and the root  
 141 mean square errors (RMSEs) was computed from the difference between modelled and  
 142 observed elevations. TPXO8 is an inverse tidal solution for both elevation and velocity  
 143 based on satellite altimetry and the shallow water equations, and is commonly taken as the  
 144 thruth for tidal elevations [see Egbert and Erofeeva, 2002, and [http://volkov.oce.orst.edu/tides/tpxo8\\_atlas.html](http://volkov.oce.orst.edu/tides/tpxo8_atlas.html)  
 145 for details].

146 To evaluate the sensitivity of our solutions to the lack of detail in the future bathyme-  
 147 tries, we constructed a simplified PD bathymetry having the same (lack of) detail as the

148 future bathymetries (see Fig. 1, top right panel). This case is denoted PD reduced in the  
 149 following, and it is the simulation we use as a benchmark for the evolution of the tide.  
 150 In PD reduced any water currently shallower than 200 m was set to 200 m. PD oceanic  
 151 ridges were smoothed out and set to have a peak depth of 2500 m and a total width of  
 152 5° degrees over which the ridge approaches the depth of the deep ocean linearly, whereas  
 153 subduction zones were set to be 1° wide and 6000 m deep with a triangular cross-section.  
 154 The remaining ocean was set to a depth computed to conserve the ocean's present day  
 155 total volume. The same values were used in the construction of the future bathymetries  
 156 shown in Fig. 1.

### 157 **2.2.2 Future bathymetries**

158 We used GPlates for the kinematic tectonic modelling of the future scenario [see  
 159 *Qin et al.*, 2012; *Duarte et al.*, 2018, and <https://www.gplates.org/> for a description].  
 160 The continental polygons provided in the GPlates data repository were used as the start-  
 161 ing point for the present day ocean, as in *Matthews et al.* [2016]. The drift paths of the  
 162 continental plates were constrained for the first 25 Myr by the drift velocities in *Schellart*  
 163 *et al.* [2007]. For the remaining 225 Myr, we used the PD globally averaged plate velocity  
 164 of 5.6 cm yr<sup>-1</sup> [see *Duarte et al.*, 2018, for a summary], but applied deviations from the  
 165 average based on the observations in *Zahirovic et al.* [2016]. The plate- and land bound-  
 166 aries from the model were output as digital greyscale images, which were used to build  
 167 the model bathymetries based on the details given for the PD sensitivity bathymetry.

### 168 **2.3 Dissipation computations**

169 The computation of tidal dissipation rates,  $D$ , was done following *Egbert and Ray*  
 170 [2001] and thus given by

$$D = W - \nabla \cdot P. \quad (5)$$

171 Here,  $W$  is the work done by the tide-generating force and  $P$  is the energy flux given by

$$W = g\rho\langle \mathbf{U} \cdot \nabla(\eta_{SAL} + \eta_{EQ}) \rangle \quad (6)$$

$$P = g\langle \eta \mathbf{U} \rangle \quad (7)$$

172 where the angular brackets mark time-averages over a tidal period.



### 3 Results

#### 3.1 Present Day sensitivity

The PD control simulation (Fig. 2, top left) has an RMSE of 11 cm when compared to TPXO8; the same computation for the reduced M2 tide give 23 cm. The K1 RMSE are 2 cm for PD and 10 cm for PD reduced, respectively. As discussed above, we did a series of sensitivity simulations for both bathymetries in which the tidal conversion coefficient was changed within a factor of 2, and the RMSE and dissipation rates did not change sig-

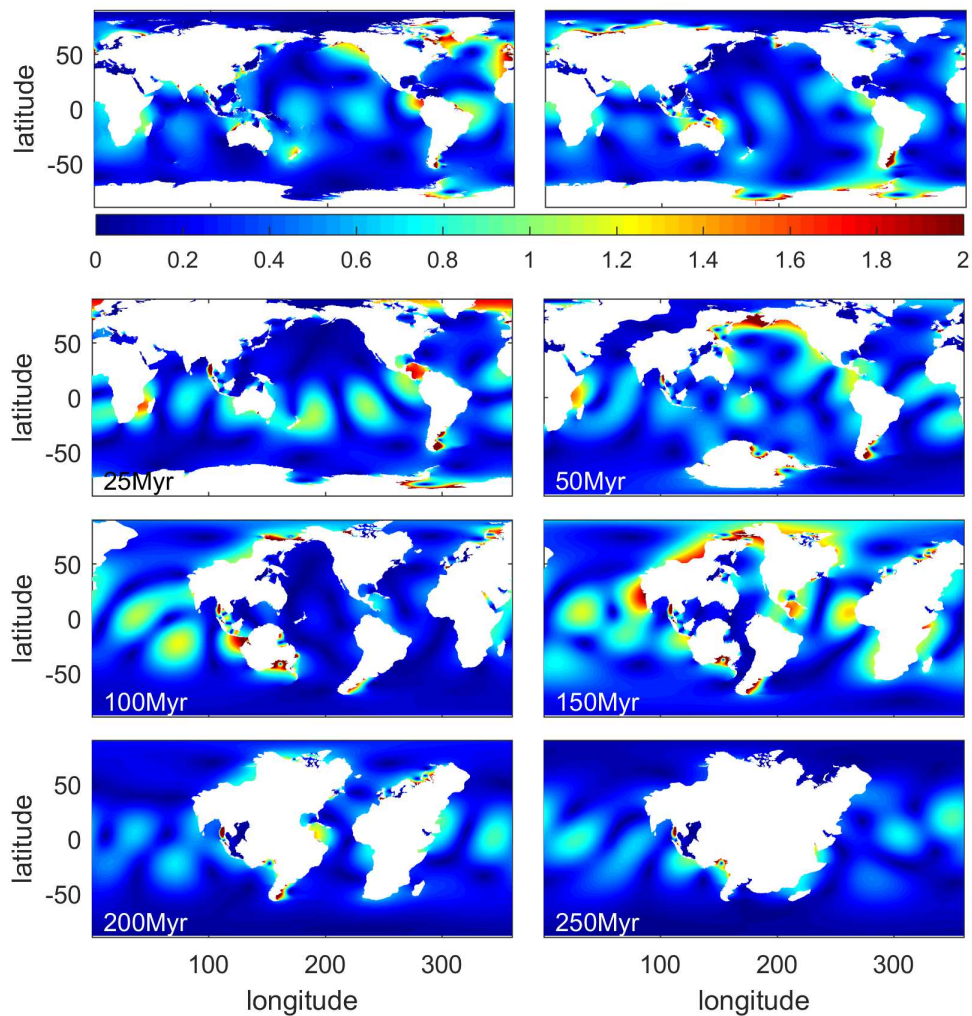


**Figure 2.** Shown are the M2 tidal amplitudes, in meters, for the PD (top left) and PD reduced (top right) simulations, along with the future time slices. Note that the colour scale saturates in the more energetic scenarios.

183 nificantly (not shown). *Green and Huber* [2013] and *Green et al.* [2017] did an extensive  
184 series of sensitivity simulations and came to the same conclusion. Consequently, we have  
185 confidence in the robustness of our results, and we have a well-constrained error bound on  
186 the simulations.

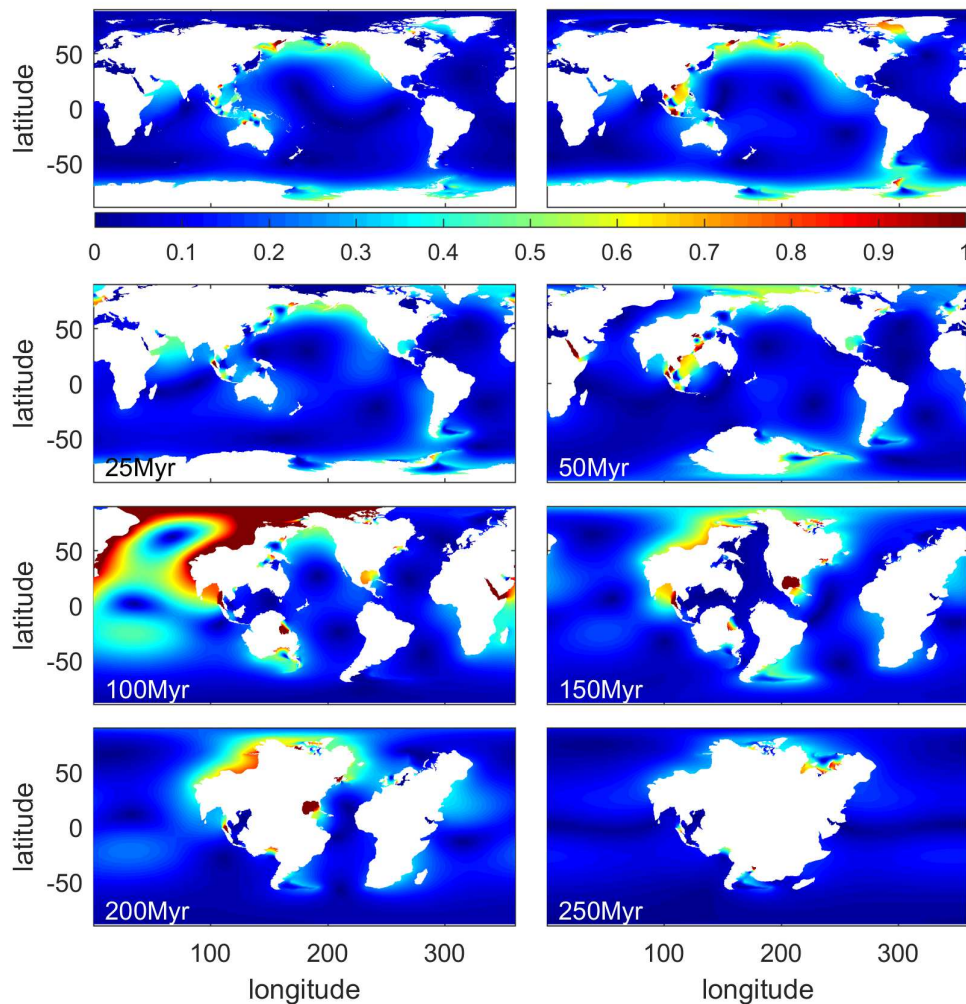
189 The PD sensitivity simulation reveals a less energetic global tide (Fig. 2, top right),  
190 with reduced M2 tidal amplitudes in the Atlantic and the emergence of fairly large M2  
191 tides along the Siberian shelf and around Antarctica. The new tides along the northern  
192 coast of Eurasia are due to the sub-arctic seas being deeper, allowing the tide to propagate  
193 into the Arctic Basin. The large PD Atlantic tides are reduced because of the water-world  
194 like ocean and reduced shelf sea area, leading to a more equilibrium-like tide [see *Eg-*  
195 *bert et al.*, 2004, for a discussion]. The weaker M2 tide in the PD reduced scenario means  
196 that we are potentially underestimating the M2 amplitudes for all future scenarios. For  
197 K1 we see a different pattern in Fig. 3 (top row panels): our synthetic bathymetry ap-  
198 pears to produce a larger K1 amplitude than the PD bathymetry. This is likely because  
199 the changed water depth allow the K1 tide to be nearer resonance in some areas, such as  
200 around Greenland and Indonesia. It is thus possible that we are overestimating K1 in the  
201 future scenarios. Note that this is a reversed response to that in *Green et al.* [2017], where  
202 their simplified bathymetry gives an enhanced M2 tide. The bathymetries in *Green et al.*  
203 [2017], however, have more topographic detail, especially in shallow water, than the ones  
204 used here. For clarity, we will describe our globally averaged or integrated metrics in rel-  
205 ative terms by normalising by the respective values from the simplified PD bathymetry.

### 207 **3.2 Tidal amplitudes**

214 The global M2 tidal amplitude increases slightly over the next 50 Myr (refer to  
215 Fig. 2 and Fig. 4a for the following discussion) due to an enhanced tide in the North At-  
216 lantic and Pacific at 25 Myr, followed by a very large Pacific tide at 50 Myr. This is be-  
217 cause the equatorial Pacific becomes half-wavelength resonant at these ages. At 100 Myr,  
218 there are large tides in the newly formed Pan-Asian Ocean (in the Asian rift) and in the  
219 Indian Ocean. This signal persists to 150 Myr when the Atlantic comes back into reso-  
220 nance to form the next tidal maximum. After 150 Myr, there is a decline of the global  
221 amplitudes as the new supercontinent starts to come together and the resonant properties

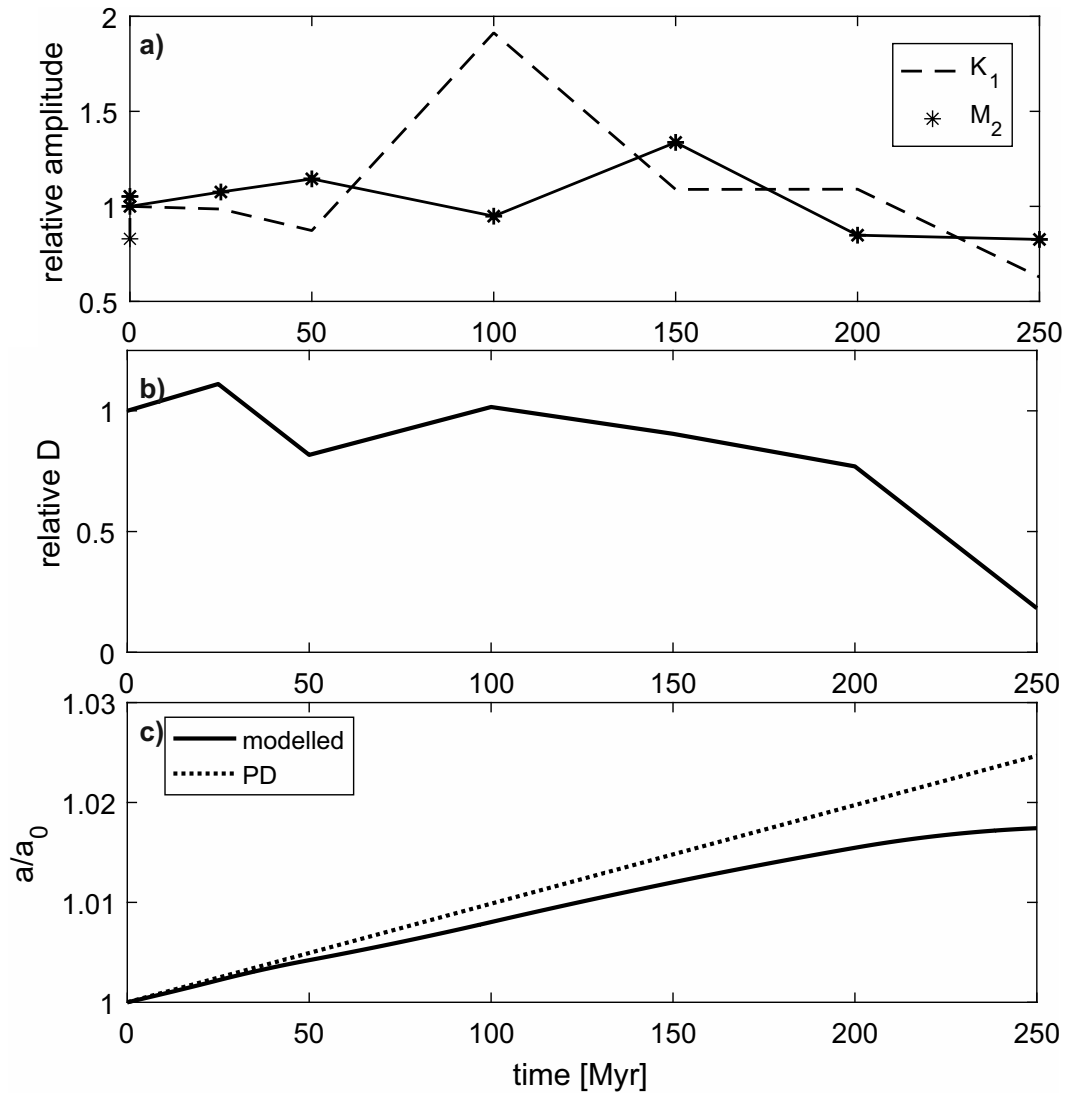
222 of the basins are lost. When Aurica has formed fully at 250 Myr, we only see large tides  
 223 locally, in embayments with a geometry allowing for local resonances.

224 K1 follows a different pattern to M2, with a global tidal maximum when M2 hits a  
 225 minimum at 100 Myr (the maximum K1 amplitude is then about 5 m). The average K1  
 226 amplitude remains relatively constant between 150–200 Myr, before a very sharp decline  
 227 as the next continent forms (Figs. 3 and 4a). It appears that K1 does not have two res-  
 228 onances in this tectonic scenario, whereas M2 does, because it becomes resonant again  
 229 when the Atlantic closes, as well as in what is left of the Pacific at 150 Myr (Fig. 2). This



187 **Figure 3.** As in Fig. 2, but showing K1 amplitudes (again in meters). Note the different color scale between  
 188 this figure and Fig. 2.

230 makes sense from a basin size perspective: because the Atlantic continues to open for a  
 231 while before closing again, K1 will never have an opportunity to become resonant in the  
 232 Atlantic, whereas M2 will be. Because of the changing size of the Pacific, it will be reso-  
 233 nant for the K1 tide at 100 Myr only.



208 **Figure 4.** a) Shown are time series of the evolution of the tidal constituents. The solid line, with markers,  
 209 represents the globally averaged M2 amplitude, whereas the dashed line shows K1 amplitudes.  
 210 b) Globally integrated M2 tidal dissipation rates normalised with the PD dissipation.  
 211 c) The evolution of the lunar distance,  $a$ , over time using the dissipation in panel b (solid) and the PD dissi-  
 212 pation rate (dashed). Both are computed from Eqs. (8)–(9). The distance is normalised by the PD distance,  
 213  $a_0$ .

### 3.3 Dissipation and Earth-Moon evolution

Overall, the global M2 dissipation rates for the remainder of the Supercontinent cycle is 84% of the present values, or 2.2 TW (Fig. 4b). This expands the results in *Green et al.* [2017] 250 Myr into the future, and strongly suggests that Earth is presently in an M2 tidal maximum. It also suggests that the maximum has a width of 50 Myr or less, and that there will be another M2 maximum occurring during the cycle around 150 Myr from now, i.e., 100 Myr before the formation of the next supercontinent. K1, in contrast, will be resonant only once in the current cycle, at 100 Myr. This is in agreement with results for the late Silurian (430 Ma), which show more energetic tides than during the Early Devonian [400 Ma; H. Byrne, pers. comm. and *Balbus*, 2014]. Pangea, the previous supercontinent, formed around 330 Myr ago and started breaking up some 180 Myr ago. It thus seems plausible that Earth's oceans go through tidal maxima some 150–200 Myr after supercontinental break up (i.e., at present) and around 100 Myr before a supercontinent forms (i.e., during the Silurian, before Pangea, and 150 Myr into the future for Aurica).

Following the theory of lunar recession in *Waltham* [2015] and summarised in *Green et al.* [2017], the recession rate,  $\partial a/\partial t$ , can be written as

$$\frac{\partial a}{\partial t} = f a^{-5.5} \quad (8)$$

where  $f$  is the tidal factor given by

$$f = \frac{2Da^6}{m'\sqrt{\omega^2 a^3}(\Omega - \omega)} \quad (9)$$

Here,  $m' = mM/(m + M)$  is the reduced mass of the Moon ( $M = 5.972 \times 10^{24}$  kg and  $m = 7.348 \times 10^{22}$  kg are the masses of the Earth and the Moon, respectively), and  $\Omega = 7.2923 \times 10^{-5}$  s<sup>-1</sup> ( $\omega = 2.6616 \times 10^{-6}$  s<sup>-1</sup>) is the rotation rate of the Earth (Moon). Using the dissipation rates in Fig. 4b, interpolated to every 1 Myr using linear interpolation to produce a smoother curve, we obtain the result in Fig. 4c. We have also, for comparison, computed the lunar distance assuming a continuous PD dissipation rate (dashed). These results further highlight the conclusions in *Green et al.* [2017], that appropriate tidal dissipation rates should be used in investigations involving lunar recession rates or distances, especially over long periods of time. Consequently, the PD recession rate is anomalously high because of the current tidal resonance in the Atlantic, and that PD tides are a poor proxy for past or future tides over large parts of the Supercontinent cycle.

## 4 Discussion

Our results support previous ideas that the tides are at their lowest when the Earth is in the supercontinent configuration. The dissipation is then less than 40% of the PD value in our simulations. The tenure of a supercontinent varies, but both Pangaea and Rodinia, the two most recent supercontinents, maintained their formation for over 100 Myr [Rogers and Santosh, 2003]. This means that dissipation rates could remain at this very low level for long periods of time – much longer than the time-scale of its resonant peaks, which here are less than 50 Myr (see below for a tighter constraint).

This project aimed to evaluate if there is a super-tidal cycle. The results strongly suggests that the answer is yes: there is a repeated gradual change between states of high and low tidal dissipation levels over the period of Aurica forming. However, there is more than one super-tidal cycle within the Supercontinent cycle. Combined with the results in Green *et al.* [2017], who goes back to Pangea 252 Myr ago, we suggest the oceans will go through two M2 super-tidal cycles and at least one K1 cycle during the current Supercontinent cycle. Consequently, the global tides are weak for long periods of time, and then pass through several quite narrow (on geological time scales) resonances. This is because there are several Wilson cycles involved in one supercontinent cycle, and as the basins open and close there can be several super-tidal cycles associated with the Wilson Cycles. This also means that the super-tidal cycle is not necessarily in phase with the supercontinent cycle. The mechanism behind the super-tidal cycle is tidal resonance, which is set up by the continental configurations: peak resonance occurs when the continental configuration results in an ocean basin of a length that is an exact multiple of half wavelengths of the M2 tidal wave. Theoretically, one would therefore be able to predict when each basin may be resonant, without being able to provide any details of the actual magnitude. To lowest order, one can assume that the tide will be large when the natural frequency of a basin is within, say, 20% of the tidal period [see Fig. 11 in Egbert *et al.*, 2004, for a theoretical estimate]. For the present, this would give a period window of about 3 hours in which the basin is close enough to resonance to support a large tide. If the ocean is 4000 m deep and we are looking at a half-wavelength resonance, we get a range of the width of the basin in which it is resonant of about 1100 km. With a continental drift rate of 6 cm yr<sup>-1</sup>, the width of the resonant peak would then be some 18 Myr, implying that Earth is currently in the beginning of the tidal maximum. There is further support for this in our results here and in Green *et al.* [2017]. They show that the tides were weak 2 Myr before

295 present, and the 25 Myr time slice in the present paper still shows a rather large tide. This  
296 is an interesting idea worth pursuing in a future paper, which would look into the time  
297 span of the resonances in more detail by simulating more time slices between now and 25  
298 Myr.

299 Ocean basin closure is a result of consumption of oceanic plate at subduction zones  
300 within the basin and sea floor spreading in a neighbouring basin. This means that there  
301 are long periods where the direction of closure is mostly fixed, with two continental plates  
302 being pulled or pushed together. The observation that there are multiple peaks in tidal  
303 dissipation makes sense in this context. There will be multiple modes of resonance for  
304 each ocean basin as it reaches the dimensions that are resonant for smaller or larger mul-  
305 tiples of the tidal wavelength. The implication of these observations is that the length of  
306 a super-tidal cycle is directly related to the length of the supercontinent cycle. Conse-  
307 quently, the period of the super-tidal cycle is set by how quickly the continental config-  
308 urations moves from one resonant mode to another. There are of course other factors that  
309 contribute to the total tidal dissipation, such as sea level changes and variations in the ex-  
310 tent of continental shelves, but through this study we have a clear indication that changing  
311 the position of the continents alone is enough to elicit significant changes in the energy  
312 of the tidal system. However, if an ocean basin is close to resonance it is much more sen-  
313 sitive to relative sea-level changes and/or continental shelf configurations than when its  
314 not in a near-resonant state. This was the case for the Last Glacial Maximum (21–18 kyr)  
315 where *Green et al.* [2017] find the largest M2 amplitude in their 252 Myr time series. This  
316 exceptionally large tide is explained by a low-stand in sea-level, exposing the dissipative  
317 shelf seas [*Egbert et al.*, 2004; *Wilmes and Green*, 2014].

318 The results here are promising, and further investigations will focus on other tec-  
319 tonic scenarios and increasing the temporal resolution of our simulations. This will pro-  
320 vide a further understanding of the future Earth system, and will, along with more sim-  
321 ulations of the past, allow us to build a better picture of the variability in tides and tidal  
322 dissipation rates over long time periods.

### 323 **Acknowledgments**

324 JAMG acknowledges funding from the Natural Environmental Research Council through  
325 grants NE/F014821/1 and NE/I030224/1. JCD acknowledges an FCT Researcher contract,  
326 an exploratory project grant Ref. IF/00702/2015, and the FCT-project UID/GEO/50019/2013-

327 IDL. HSD was supported by FCT (ref. UID/GEO/50019/2013 - Instituto Dom Luiz; FCT  
 328 PhD grant, ref. PD/BD/135068/2017). Kara Matthews (Oxford University) provided in-  
 329 valuable support on using GPlates. Comments from Sophie Wilmes, Jeroen Ritsema (edi-  
 330 tor), Dietmar Müller (reviewer), and an anonymous reviewer greatly improved the manuscript.  
 331 The data is available from the Open Science Framework ([osf.io/8ydwv](https://osf.io/8ydwv)).

## 332 **References**

- 333 Arbic, B. K., and C. Garrett (2010), A coupled oscillator model of shelf and ocean tides,  
 334 *Continental Shelf Research*, 30, 564–574.
- 335 Balbus, S. A. (2014), Dynamical, biological and anthropic consequences of equal lunar  
 336 and solar angular radii, *Proceeding of the Royal Society of London, A*, 470, 20140,263.
- 337 Boschman, L. M., and D. J. J. van Hinsbergen (2016), On the enigmatic birth of the Pa-  
 338 cific Plate within the Panthalassa Ocean, *Science Advances*, 2, e1600,022.
- 339 Bradley, D. (2011), Secular trends in the geologic record and the supercontinent cycle,  
 340 *Earth-Science Reviews*, 108, 16–33.
- 341 Burke, K. (2011), Plate tectonics, the wilson cycle, and mantle plumes: Geodynamics  
 342 from the top, *Annual Review of Earth and Planetary Sciences*, 39, 1–29.
- 343 Burke, K., and J. F. Dewey (1974), Hot spots and continental breakup: implications for  
 344 collisional orogeny, *Geology*, 2, 57–60.
- 345 Duarte, J., W. Schellart, and F. Rosas (2018), The future of earth's oceans: Consequences  
 346 of subduction initiation in the atlantic and implications for supercontinent formation,  
 347 *Geological Magazine*, 155, 45–58.
- 348 Egbert, G. D., and S. Erofeeva (2002), Efficient inverse modeling of barotropic ocean  
 349 tides, *Journal of Atmospheric and Oceanic Technology*, 19, 183–204.
- 350 Egbert, G. D., and R. D. Ray (2001), Estimates of M2 tidal energy dissipation from  
 351 Topex/Poseidon altimeter data, *Journal of Geophysical Research*, 106, 22,475–22,502.
- 352 Egbert, G. D., B. G. Bills, and R. D. Ray (2004), Numerical modeling of the global  
 353 semidiurnal tide in the present day and in the last glacial maximum, *Journal of Geo-*  
 354 *physical Research*, 109, C03,003, doi: 10.1029/2003JC001,973.
- 355 Golonka, C. R. (1991), Jurassic and cretaceous plate tectonic reconstructions, *Paleogeog-*  
 356 *raphy, Palaeoecology, Palaeoclimatology*, 87, 493–501.
- 357 Golonka, J. (2007), Late triassic and early jurassic palaeogeography of the world, *Paleo-*  
 358 *geography, Palaeoecology, Palaeoclimatology*, 244, 297–307.



- 359 Green, J., M. Huber, D. Waltham, J. Buzan, and M. Wells (2017), Explicitly modeled  
 360 deep-time tidal dissipation and its implication for lunar history, *Earth and Planetary*  
 361 *Science Letters*, *461*, 46–53.
- 362 Green, J. A. M. (2010), Ocean tides and resonance, *Ocean Dynamics*, *60*, doi:  
 363 10.1007/s10236-010-0331-1.
- 364 Green, J. A. M., and M. Huber (2013), Tidal dissipation in the early Eocene and implica-  
 365 tions for ocean mixing, *Geophysical Research Letters*, *40*, doi:10.1002/grl.50,510.
- 366 Griffiths, S. D., and W. R. Peltier (2008), Megatides in the Arctic Ocean under glacial  
 367 conditions, *Geophysical Research Letters*, *35*, L08,605, doi:10.1029/2008GL033,263.
- 368 Hendershott, M. C. (1977), Numerical models of ocean tides, in *The Sea vol. 6*, pp. 47–89,  
 369 Wiley Interscience Publication.
- 370 Herold, N., M. Huber, R. D. Mäijller, and M. Seton (2012), Modeling the miocene cli-  
 371 matic optimum: Ocean circulation, *Paleoceanography*, *27*, PA1209.
- 372 Kagan, B., and A. Sundermann (1996), Dissipation of tidal energy, paleotides, and evolu-  
 373 tion of the earth-moon system, *Advances in Geophysics*, *38*, 179–266.
- 374 Matthews, K., K. Maloney, S. Zahirovic, S. Williams, M. Seton, and R. D. Mäijller  
 375 (2016), Global plate boundary evolution and kinematics since the late paleozoic, *Global*  
 376 *and Planetary Change*, *146*, 226–250.
- 377 Müller, R. D., M. Sdrolias, C. Gaina, and W. R. Roest (2008), Age, spreading rates, and  
 378 spreading asymmetry of the world’s ocean crust, *Geochemistry, Geophysics, Geosystems*,  
 379 *9*, Q04006.
- 380 Nance, R. D., T. R. Worsley, and J. B. Moody (1988), The supercontinent cycle, *Scientific*  
 381 *American*, *256*, 72–79.
- 382 Pelling, H. E., and J. A. M. Green (2013), Sea-level rise, tidal power, and tides in the Bay  
 383 of Fundy, *Journal of Geophysical Research*, *118*, 1–11.
- 384 Platzman, G. W. (1975), Normal modes of the Atlantic and Indian Oceans, *Journal of*  
 385 *Physical Oceanography*, *5*, 201–221.
- 386 Qin, X., R. Muller, J. Cannon, T. Landgrebe, C. Heine, R. Watson, and M. Turner (2012),  
 387 The gplates geological information model and markup language, *Geoscientific Instru-*  
 388 *mentation, Methods and Data Systems*, *1*, 111–134.
- 389 Rogers, J., and M. Santosh (2003), Supercontinents in earth history, *Gondwana Research*,  
 390 *6*, 357–368, doi:10.1016/S1342-937X(05)70993-X.

- 391 Schellart, W. P., J. Freeman, D. R. Stegman, L. Moresi, and D. May (2007), Evolution and  
392 diversity of subduction zones controlled by slab width, *nature*, *446*, 308–311.
- 393 Stammer, D., R. D. Ray, O. B. Andersen, B. K. Arbic, W. Bosch, L. CarrÁÍre, Y. Cheng,  
394 D. S. Chinn, B. D. Dushaw, G. D. Egbert, S. Y. Erofeeva, H. S. Fok, J. A. M. Green,  
395 S. Griffiths, M. A. King, V. Lapin, F. G. Lemoine, S. B. Luthcke, F. Lyard, J. Morison,  
396 M. MÄijller, L. Padman1, J. G. Richman, J. F. Shriver, C. K. Shum, E. Taguchi, and  
397 Y. Yi (2014), Accuracy assessment of global ocean tide models, *Reviews of Geophysics*,  
398 *52*, doi:10.1002/2014RG000,450.
- 399 Waltham, D. (2015), Milankovitch period uncertainties and their impact on cyclostratigra-  
400 phy, *Journal of Sedimentary Research*, *85*, 990–998.
- 401 Wilmes, S.-B., and J. A. M. Green (2014), The evolution of tides and tidally  
402 driven mixing over 21,000 years, *Journal of Geophysical Research*, *119*,  
403 doi:10.1002/2013JC009,605.
- 404 Wilson, J. T. (1966), Did the Atlantic Close and then Re-Open? *Nature*, *211*, 676–681.
- 405 Yoshida, M., and M. santosh (2011), Future supercontinent assembled in the northern  
406 hemisphere, *Terra Nova*, *23*, 333–338.
- 407 Zahirovic, S., K. J. Matthews, N. Flament, R. D. Müller, K. C. Hill, M. Seton, and  
408 M. Gurnis (2016), Tectonic evolution and deep mantle structure of the eastern tethys  
409 since the latest jurassic, *Earth-Science Reviews*, *162*, 293–337.
- 410 Zaron, E. D., and G. D. Egbert (2006), Estimating open-ocean barotropic tidal dissipation:  
411 The Hawaiian Ridge, *Journal of Physical Oceanography*, *36*, 1019–1035.